Available online at www.sciencedirect.com
ScienceDirect
Icarus 189 (2007) 523–537
ICARUS
www.elsevier.com/locate/icarus

Aggregate impacts in Saturn's rings

Raine Karjalainen *

Department of Physical Sciences, Astronomy Division, P.O. Box 3000, FIN-90014, University of Oulu, Finland

Received 6 November 2006; revised 16 February 2007

Available online 12 March 2007

Abstract

Ring particle aggregates are formed in the outer parts of Saturn's main rings. We study how collisions between aggregates can lead to destruction or coalescence of these aggregates, with local N-body simulations taking into account the dissipative impacts and gravitational forces between particles. Impacts of aggregates with different mass ratios are studied, as well as aggregates that consist of particles with different physical properties. We find that the outcome of the collision is very sensitive to the shape of the aggregate, in the sense that more elongated aggregates are more prone to be destroyed. We were interested in testing the accretion criterion Barbara and Esposito [Barbara, J.M., Esposito, L.W., 2002. Icarus 160, 161–171] used in their F ring simulations, according to which accretion requires that the masses of the colliding bodies differ at least by a factor of 100. We confirm that such a critical mass ratio exists. In particular, simulations indicate that the exact critical mass ratio depends on the internal density and elasticity of particles, and the distance from the planet. The zone of transition, defined by the distance where individual particles or small aggregates first start to stick on the larger aggregate, and by the distance where two similar sized aggregates on the average eventually coalesce is only about 5000 km wide, if fixed particle properties are used. The rotational state of the aggregates that form via aggregate collision rapidly reaches synchronous rotation, similarly to the aggregates that form via gradual growth.

Keywords: Accretion; Saturn, rings

1. Introduction

Two images taken by Cassini Imaging Science Subsystem revealed 'propeller'-shaped features in the A ring that are interpreted to be caused by embedded moonlets with 40–120 m in diameter (Tiscareno et al., 2006). The nature of these objects is still unclear as they could be either moonlet fragments held together by internal strength or gravitationally bound particle aggregates. Also Cassini UVIS stellar occultation observations of the F ring have shown 9 events ranging in size from 30 to 600 m along the occultation track, interpreted as aggregates (Meinke et al., 2006).

Numerical simulations have also indicated that the outer parts of Saturn's main rings are an environment where ring particles may stick together to form particle aggregates due to gravity (Salo, 1992b, 1995; Karjalainen and Salo, 2004). The 'propeller' structures had been already predicted with numerical simulations, for example by Seiß et al. (2005).

In Karjalainen and Salo (2004), we studied the onset of growth of aggregates via gravitational sticking of small particles and as a result we could estimate the radial distance beyond which aggregates start to form and the timescales for accretion. Now we made these aggregates to collide with each other to find out if they will accrete or be destroyed.

Destruction of ring particle aggregates could in principle be explained with tidal stresses, rotational stresses, or by collisions between the aggregates (see Weidenschilling et al., 1984). Tidal accelerations are $\sim\Omega^2 r$, where Ω is the orbital frequency and r is the aggregate radius; rotation induces an additional acceleration $\sim\omega^2 r$, where ω is the rotation rate of the aggregate, whereas aggregate self-gravity is proportional to $G\rho r$, where G is the gravitational constant and ρ is the internal density of the aggregate. Rotational stresses dominate if the aggregate's spin period is shorter than its orbital period, while tidal stresses are dominant otherwise. Rotational stresses are probably ruled out as ω is not expected to get high enough during the growth of

* Fax: +358 8 553 1934.
E-mail address: raine.karjalainen@oulu.fi.

0019-1035/$ – see front matter
doi:10.1016/j.icarus.2007.02.009

the aggregate (Morishima and Salo, 2004). Tidal stresses are not a likely explanation for destruction, as the numerical simulations of Karjalainen and Salo's (2004) paper indicate that the aggregate density seems to stay fixed during its growth (at least over the limited growth accessible via direct particle simulations). In this case, gravitational, tidal and rotational forces all increase proportionally to the size of the growing aggregate. Mutual collisions of aggregates or collisions between an aggregate and the largest individual particles seem thus to offer one natural candidate for the destruction of aggregates.

Collisions between the aggregates in outer parts of Saturn's rings have been suggested to be related both to the existence of the F ring and to the transient brightening events seen in the F ring. Cuzzi and Burns (1988) introduced the presence of a population of moonlet scale objects (0.1–10 km radius) extending throughout the entire annulus between the F ring shepherds. According to them the F ring may be the consequence of a relatively recent collision between two of the largest moonlets.

Re-analyzing the Voyager data revealed that there are transient brightenings in the F ring (Showalter, 1998, 2004). According to Showalter's model micro-meteoroids hit the moonlets and thus small particles are lifted from their surfaces, leading to local brightenings. Evidence for particle aggregation comes also from Poulet et al. (2000) as they analyzed transient F ring features observed during 1995 Earth and Sun crossing of Saturn's ring plane. They proposed that these features might be clouds of ejecta produced by collisions where large parent bodies of the F ring are involved. Barbara and Esposito (2002) gave an alternative model to Showalter's but similar to Poulet et al. (2000) explaining the brightenings by moonlets colliding with each other. Unlike Poulet et al. (2000) Barbara and Esposito took into account the size distribution of the moonlets. They criticize Showalter's (1998) model due to non-detection of smaller events. According to their model, if moonlets that collide have a mass ratio higher than ∼100, this will lead to accretion, otherwise the result is a disruption. They got their critical mass ratio from Canup and Esposito (1995) who made similar simulations suggesting that accretion results only from collision of those bodies whose masses differ substantially depending on coefficient of restitution. Canup and Esposito made simulations in the broad "tidally modified" region surrounding the classical Roche limit. Barbara and Esposito track probabilities of mass transfer for binned intervals of an initially continuous mass distribution. The mass ratio deciding the outcome of the collision between aggregates can be tested by N-body simulations as we show in this paper.

According to Ohtsuki's (1993) three-body integrations of particle orbits in planetary rings, the accretion probability of two solid spherical bodies is determined by the r_p-parameter, i.e., the ratio of the sum of the particle radii to the gravitational, or the Hill radius of the pair, $r_\mathrm{p} = (r_1 + r_2)/R_\mathrm{H}$, where $R_\mathrm{H} = a(m_1 + m_2)^{1/3}/(3M)^{1/3}$, and r_1, r_2, m_1, and m_2 are the radii and masses of the small particles rotating about the central object with mass M at distance a. The r_p can also be written as

$$r_\mathrm{p} = \left(\frac{9}{4\pi}\right)^{1/3} \rho^{-1/3} M^{1/3} a^{-1} \frac{1+\mu^{1/3}}{(1+\mu)^{1/3}}, \tag{1}$$

showing explicitly the dependence of r_p on the mass ratio between the particles, denoted as $\mu = m_2/m_1$. According to Ohtsuki (1993), with $r_\mathrm{p} \geqslant 1$ accretion by gravitational force is prohibited, with $2/3 < r_\mathrm{p} < 1$ accretion may be possible but is quite difficult, and with $r_\mathrm{p} \leqslant 2/3$ particles are completely inside their Hill surface and there is almost always accretion unless relative velocity is too high and/or if the elasticity model is nearly elastic. This idealized three-body criterion in mind we wanted to see how this holds with two aggregates colliding.

In Karjalainen and Salo (2004), we made a short survey of the rotation and shape of gravitationally bound particle aggregates forming in simulations (see Karjalainen and Salo, 2004, Fig. 12). This is now examined somewhat more in detail as we study the rotation and the shape of the aggregate that has formed after the collision of aggregates, whereas in Karjalainen and Salo (2004) only aggregates formed via gradual accretion were studied.

We do not take into account adhesion (Albers and Spahn, 2006) and if it is important, besides gravity, it could also be a significant factor in accretion and destruction of aggregates.

In Section 2 the N-body method is briefly described, in Section 3 the specifics of the aggregate and the collision of two aggregates are discussed. In Section 4 are the results for colliding the aggregates. Conclusions and discussion together with some ideas of future work are found in Section 5.

2. N-body simulation method

We are using the local simulation method (Wisdom and Tremaine, 1988; Salo, 1991, 1992a, 1992b, 1995; Karjalainen and Salo, 2004) to study the collision-induced destruction and accretion of ring particle aggregates. Both collisions and gravitational interactions are taken into account. As in Karjalainen and Salo (2004), all calculations are restricted to a small comoving region inside the ring. The calculation area is at the distance a from the planet and is moving with the circular angular velocity Ω. The systematic shear in the radial direction is taken into account via periodic boundary conditions. Linearized equations of motion are employed, for the $i = 1, \ldots, N$ particles with position vectors $\vec{R}_i \equiv (x_i, y_i, z_i)$ and masses m_i,

$$m_i\left(\ddot{x}_i - 2\Omega\dot{y}_i - 3\Omega^2 x_i\right) = F_x^\mathrm{g} + F_x^\mathrm{imp}, \tag{2}$$

$$m_i(\ddot{y}_i + 2\Omega\dot{x}_i) = F_y^\mathrm{g} + F_y^\mathrm{imp}, \tag{3}$$

$$m_i\left(\ddot{z}_i + \Omega^2 z_i\right) = F_z^\mathrm{g} + F_z^\mathrm{imp}, \tag{4}$$

where the x-axis is pointing towards the radial direction, the y-axis towards the direction of the mean orbital motion, and the z-axis completes the right-handed coordinate system. Equations (2)–(4) above are valid when $x/a \ll 1$, $y/a \ll 1$, $z/a \ll 1$, which conditions are certainly fulfilled in rings.

Mutual gravitational forces

$$\vec{F}_i^\mathrm{g} = \sum_{\substack{j=1 \\ j\neq i}}^{N} -Gm_i m_j \frac{\vec{R}_{ij}}{r_{ij}^3}, \tag{5}$$

where $\vec{R}_{ij} \equiv \vec{R}_i - \vec{R}_j$ and $r_{ij} \equiv |\vec{R}_{ij}|$. Due to the relatively small number of simulation particles we calculate the self-gravity by direct summation over all particle pairs.

For the modeling of impacts the force model introduced by Salo (1995) is used. All particles are treated as indestructible uniform spheres. According to Bridges et al. (2001) the impact durations are $\lesssim$1 s. Instead, we use impact durations that are about 50 times longer. This way the total number of simulation steps is reduced significantly, still keeping the impact duration short enough to keep the coefficient of restitution ϵ_n from deviating significantly from realistic values, due to orbital motion or self-gravity during the prolonged impact. The impact force is divided into normal and tangential components

$$\vec{F}^{\rm imp} = F_n \hat{c} + F_t \hat{c}_t, \tag{6}$$

where $\hat{c} = (\vec{R} - \vec{R}')/|\vec{R} - \vec{R}'|$ is the unit vector in the direction between the particle centers, and $\hat{c}_t$ is the unit vector in the direction of the component of the instantaneous velocity difference along the tangent plane of impact.

Most of the simulations use a velocity-dependent normal coefficient of restitution

$$\epsilon_n(v_n) = \max\left[\left(\frac{v_n}{v_c}\right)^{-0.234}, 0.25\right], \tag{7}$$

this is true when $v_n > v_c$, otherwise $\epsilon_n(v_n)$ is set to unity. Bridges et al.'s (1984) laboratory measurements show that $v_c \approx 0.0077\ \mathrm{cm\,s^{-1}}$ in the case of low temperature frost-covered ice.

As in Karjalainen and Salo (2004), surface friction is included in some simulations. We model friction by assuming that the tangential component of force between the colliding particles is proportional to the normal force,

$$F_t = -k_f F_n, \tag{8}$$

where $k_f \geqslant 0$ is the coefficient of friction. Friction related laboratory measurements are for tangential coefficient of restitution ϵ_t. Comparing the total change of tangential and normal velocity components in impacts, $v_t = |\vec{v}_{\rm coll} - \vec{v}_n|$ and $v_n = |\vec{v} \cdot \vec{c}|$, one gets

$$k_f = \frac{2}{7}\frac{(1-\epsilon_t)v_t}{(1+\epsilon_n)v_n}, \tag{9}$$

see Karjalainen and Salo (2004). The relation between k_f and ϵ_t thus depends on the direction of the impact. Supulver et al. (1995) get $\epsilon_t \approx 0.9$ for glancing 1 $\mathrm{cm\,s^{-1}}$ impacts of ice particles, suggesting quite a small k_f of the order of 0.01–0.1.

We also wanted to explore the effect of including a size distribution on the outcome of aggregate collisions. We use a power-law size distribution for the particles making the aggregate,

$$\mathrm{d}N/\mathrm{d}r \sim r^{-q}, \tag{10}$$

where $q = 3$ and $0.5 < r < 5.0$ m. Voyager I radio occultation measurements revealed the size distribution to be of this kind but with a smaller lower cut-off $\sim$1 cm (Marouf et al., 1983). Our larger lower cut-off is due to computational reasons. Even though the width used for the size distribution is narrower than that observed, it mimics quite well the dynamical behavior of the aggregate collision, as the most of the ring mass is in the large particles.

Two main types of simulations are conducted: (1) accretion simulations for a large range of distances, (2) aggregate collision experiments, using different mass ratios and physical properties of particles, for three different distances 135,000, 140,000, and 145,000 km, which cover the interesting region for solid ice particles with $\rho = 900\ \mathrm{kg\,m^{-3}}$.

The aggregates we use in our impact experiments were made in a similar fashion as in Karjalainen and Salo (2004), forming at different distances via gradual growth. The number of simulation particles ranges from 50 to 5500. The time interval of gravity updates, ΔT, is 0.001 (in orbital periods) and the spring constant in modeling collisions, ω_0/Ω, is the same as in the standard case of Karjalainen and Salo (2004), corresponding to typical impact duration of 1/800 orbital periods. The collisions are modeled with a velocity-dependent coefficient of restitution $\epsilon_n(v_n)$, and there is no friction in our standard model ($k_f = 0$). The internal density ρ of the particles making the aggregates is 900 $\mathrm{kg\,m^{-3}}$. Note that although dimensional numbers are used in our simulations (see Eqs. (2)–(4)) we will present most of our results also in non-dimensional Hill units. This will make it easy to scale our results for different internal densities.

3. Simulating the collision between ring particle aggregates

Our main interest is in the outcome of the collision between two particle aggregates. What happens to the target aggregate? After the collision, in some cases there are some ejecta particles, which rapidly drift away from the main aggregates due to Keplerian shear. Due to the periodic boundary conditions of the simulation method there is a possibility that these particles might collide again with the target aggregate or the remains of it. We eliminate this possibility by removing the periodic boundaries in the aggregate impact simulations (they are thus applied only in simulations for forming the aggregates, as in Karjalainen and Salo, 2004).

For two particles or aggregates to collide in the gravitational environment as in Saturn's rings they need to have a certain initial radial distance difference. Otherwise, they end up in horseshoe orbits if the radial distance difference is too small, or just pass by each other if the radial distance difference is too big. See Fig. 1 for the orbits near the aggregate.

A convenient way to scale impact calculations for particles orbiting a central mass is to use the Hill-scaling like Ida and Nakazawa (1989), who studied the collisions between planetesimals in the solar gravity field. They studied the orbits where collisions can occur; i.e., they concentrated only to a certain radial distance region denoted by impact parameter

$$b = \frac{a^* - a_0^*}{h a_0^*}, \tag{11}$$

where a_0^* is the semimajor axis of the orbit of the protoplanet (in our case semimajor axis of the orbit of the target aggregate),

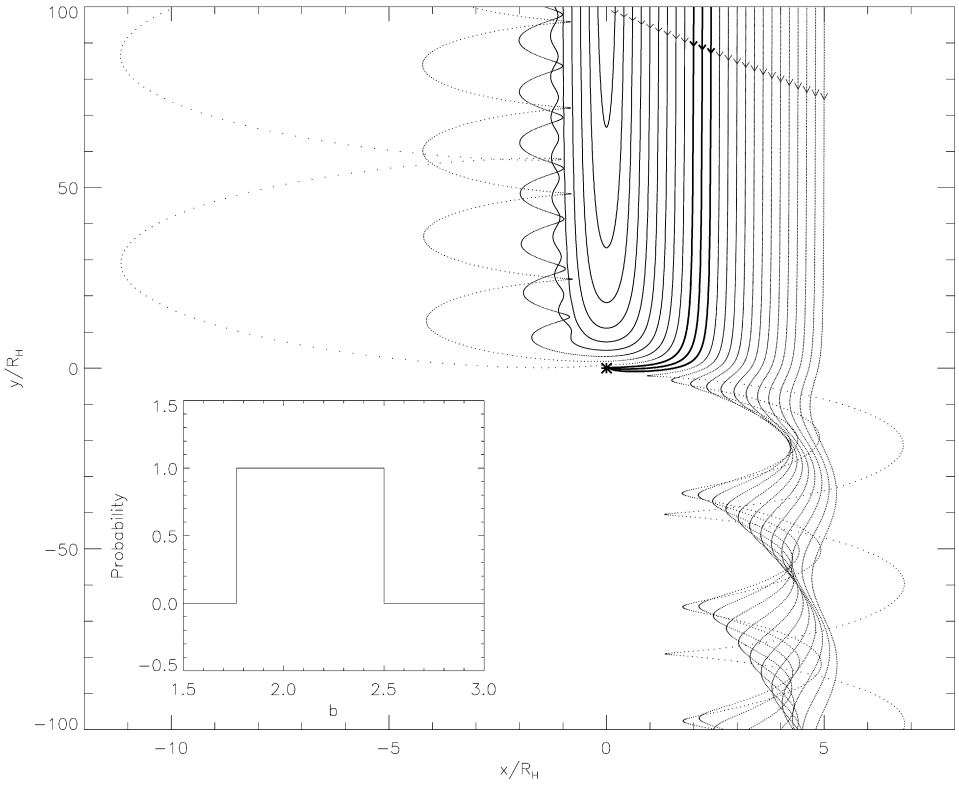

Fig. 1. *Schematic figure of the orbits of aggregate encounters in non-colliding and colliding orbits*. Orbits of the impactor are plotted with different impact parameters b in rotating Hill-coordinates. The planet is to the negative x direction and the orbital motion is to positive y direction. One can see the zone for horseshoe orbits, colliding orbits (indicated by thicker lines), and the orbits that pass by. The length of arrows reflects the linear increase of impactor flux with impact parameter. For clarity, only the orbits further away from the planet (for positive impact parameter) than the aggregate are shown. Had the inner orbits been included a typical 'propeller' shape would emerge (see, e.g., Murray and Dermott, 2000, p. 121). The insert shows the probability of collision as a function of impact parameter.

a^* is the semimajor axis of the impactor aggregate, and h is the reduced Hill radius

$$h = (m/3M)^{1/3}, \tag{12}$$

where M is the mass of the central object and m that of the protoplanet (in our case M corresponds to the mass of Saturn and m to the total mass of the target and the impactor aggregate). We limit our studies to circular orbits; i.e., inclination $i = 0$ and eccentricity $e = 0$. This is not as bad an assumption as it might first sound, because according to our previous simulations larger ring particles tend to have smaller i and e, and they are even smaller for aggregates.

Our simulations are made with impact parameters between $b = 1.755$ and 2.560, with the interval $\Delta b = 0.005$. Compared to Ida and Nakazawa (1989) the range of b leading to interaction is somewhat wider but almost the same as they used: $b = 1.765$–2.545. The main difference is that with three-body integrations there is no disruption; the particles either stick together after the collision or separate. In our case with aggregates the target aggregate can survive the collision, however losing some mass in the collision. Also the accretion is different; as with aggregates made out of ring particles, there is accretion when the target aggregate's mass is more than its original mass. The maximum can reach the combined mass of the target aggregate and the impacting aggregate.

3.1. Outcomes of aggregate collisions

The range of impact parameters we choose covers, not only the orbits leading to a physical impact, but also those leading to a close encounter, which can also potentially disrupt the aggregate. There are three main types of outcomes from the collision: (1) destruction of both aggregates, (2) accretion, i.e., the aggregates merge into one bigger aggregate, or (3) one or both aggregates survive the collision but there is a population of ejecta particles. These three different possibilities are illustrated in Fig. 2. Sometimes there is a split-up of the target aggregate but that is very rare. Usually, if there are two large fragments after the impact, they are the main remainders of the target and the impactor aggregates.

The outcome of a collision between two aggregates depends strongly on the shape of the aggregates (see Fig. 3) in the sense that an elongated aggregate is much more prone to get disrupted both in a collision and in a close encounter. In contrast, for the same distance and particles' physical properties the collisions of round aggregates can lead to survival of both aggregates, or accretion of these aggregates. Since we want to study the dependence of accretion on the mass ratio and other physical properties, we need to eliminate the sporadic influence of the aggregate shape. In order to do so we will use the same aggregate shape in all our impact experiments for the distance range $a = 135{,}000$–$145{,}000$ km. We first studied the average shape

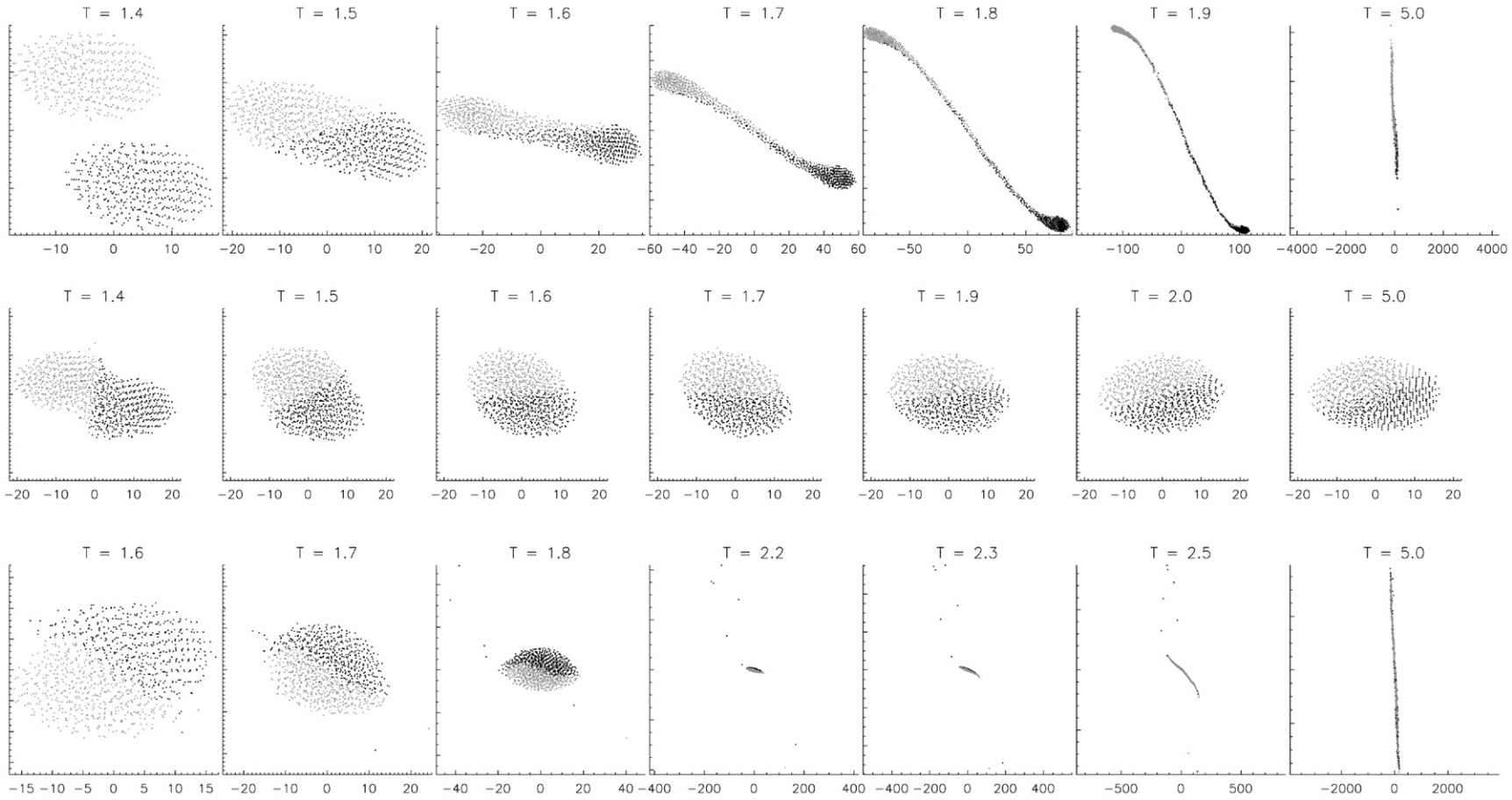

Fig. 2. *Possible outcomes of the aggregate collision*. The lowest row shows the total destruction of both aggregates. The middle row illustrates complete accretion, while in the uppermost row there is a lot of debris from the impact, although both aggregates survived the collision. Note that while the size of the displayed area is different in each case, the aspect ratio is fixed so that the radial and tangential scales are equal. Time T is in orbital periods and the scales are in meters. The distance is 140,000 km, the internal density of particles is 900 kg m^{-3} and the radii of these identical particles is 1 m. The ring particles forming the target aggregate and the impactor aggregate are displayed with different colors. The three simulations displayed are identical expect that the impact parameter is changed: b is 2.000, 2.275, and 2.500 Hill radii $R_{\rm H}$ for the cases of total disruption, accretion, and partial disruption, respectively.

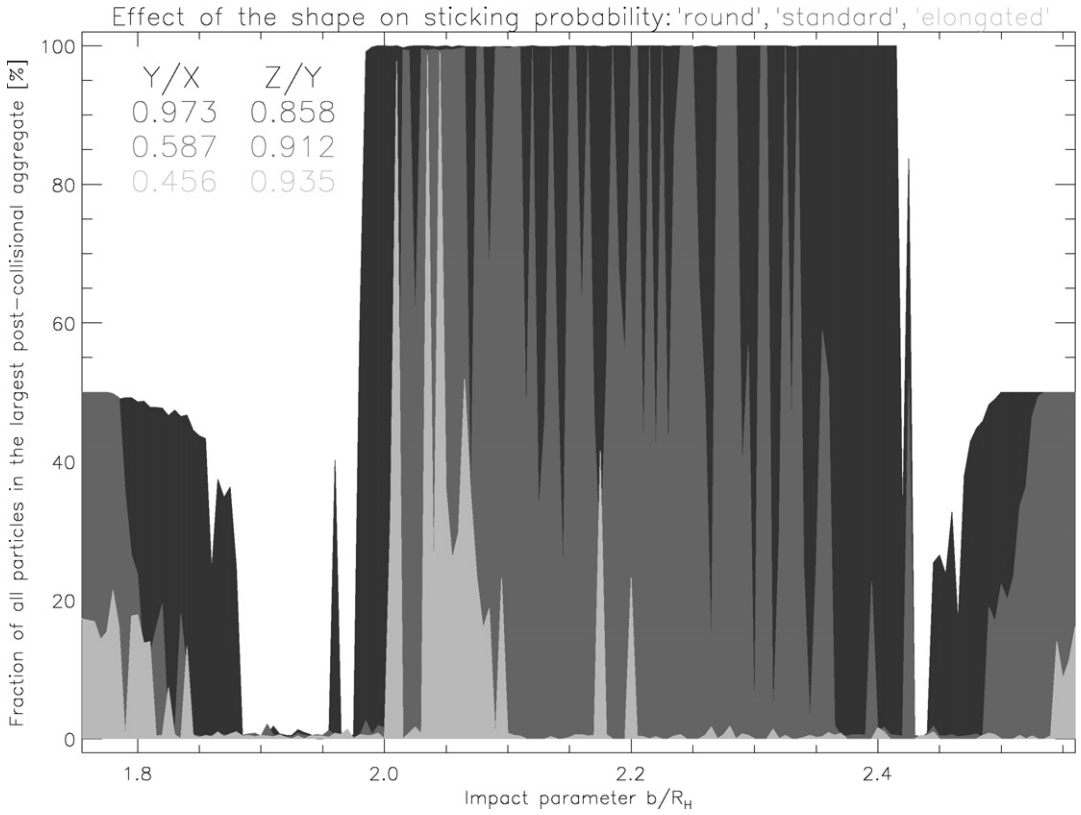

Fig. 3. *The effect of the shape of the aggregate on the collision outcome*. Gravitational aggregates with three different shapes are compared. The 'round' aggregate has $Y/X = 0.973$, $Z/Y = 0.858$, the 'elongated' has $Y/X = 0.456$, $Z/Y = 0.935$. These two are compared to the average 'standard' aggregate with $Y/X = 0.587$, $Z/Y = 0.912$. On the horizontal axis is the impact parameter b and on the vertical axis is the percentage of particles in the target aggregate after the impact. Both the target and the impactor aggregates have 500 particles in the beginning. As can be seen from $b < 1.8R_H$ and $b > 2.55R_H$, for the 'elongated' aggregate already the close encounter is enough to disrupt the aggregate.

of the aggregate formed via gradual accretion, as a function of the parameter r_p. In Karjalainen and Salo (2004, Fig. 12), we showed the shape vs r_p relation with just one simulation per r_p value, but now we have 20 simulations for each r_p and we take the average shape of those aggregates (see Figs. 4 and 5). The shape was identified by measuring the principal axes of the ellipsoid fit over the aggregates that formed (see Karjalainen and Salo, 2004). The aggregate's shape gets rounder further away from the planet, qualitatively like the Roche ellipsoid (see Fig. 4). However, between 135,000 and 145,000 km the aggregates from identical particle simulations seem to have more or less a constant shape, and enabled us to use the same target aggregate. Averaging the Y/X and Z/Y ratios for a number of aggregates we get the average shape $Y/X = 0.609$ and $Z/Y = 0.897$. Then an aggregate that was closest to this typical size was chosen as our standard aggregate (the target aggregate for all the simulations with different μ). With the $N = 500$ case the standard aggregate has $Y/X = 0.587$ and $Z/Y = 0.912$, values being within the scatter for $a = 135{,}000$–$145{,}000$ km region (see Fig. 4). For comparison, the most elongated stable self-gravitating Roche ellipsoid has $Y/X = 0.511$ and $Z/Y = 0.945$ (see Chandrasekhar, 1969, p. 189).

The mean shape for an aggregate with a size distribution is from 60 simulations that lasted for 50 orbits each, being $Y/X = 0.709$ and $Z/Y = 0.928$. Compared to the standard aggregate made of identical particles, we see that aggregates with a distribution of sizes are rounder, and have a greater filling factor, leading to a larger effective mean density. The effect of optical depth τ (and thus N) was tested with one set of simulations with 20 different seeds, for 140,000 km, $\tau = 0.5$ and with $N = 5500$. The shape, i.e., Y/X and Z/Y, for both size distribution simulation sets, $\tau = 0.25$ and $\tau = 0.5$ were within the error limits (see Figs. 4 and 5). The mean shape of an aggregate with a size distribution differs from one with identical particles, which is natural as the effective density of the aggregate is different.

The particle aggregates that form from identical particle simulations are limited by the maximum volume density of such spherical particles; that is $\pi/\sqrt{18} \approx 0.74$. Gravitational aggregates that form from our simulations are not quite this dense, as that is the theoretical maximum. For example the average volume densities for the $\tau = 0.05$: $a = 170{,}000$ km, 200,000 km and $\tau = 0.1$: 160,000 km are 0.73, 0.72, and 0.71, respectively. In the case of the size distribution the average over twenty simulations for $\tau = 0.25$, $a = 150{,}000$ km is 0.80. In Fig. 4 we have plotted the average shape of the aggregates for different distances. Curves for the Roche ellipsoids are calculated using the densities of 0.74×900, 0.80×900, and 900 kg m^{-3}; corresponding to the maximum packing density times the internal density of the particles for the identical particle aggregates and

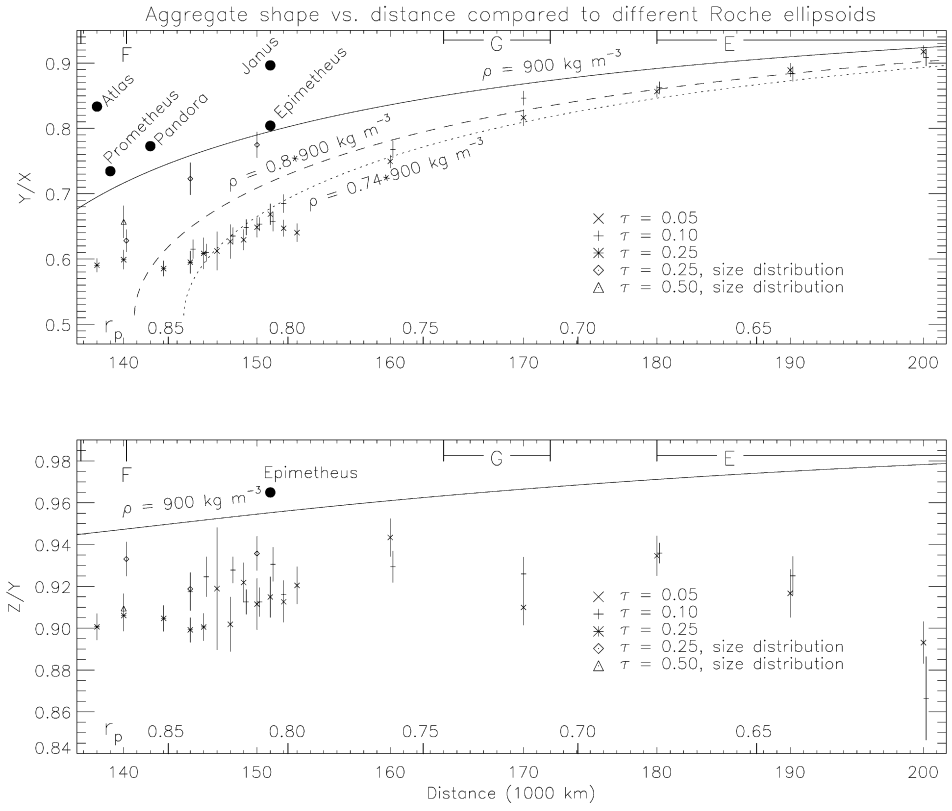

Fig. 4. *Typical shape vs distance of aggregates forming via gradual growth*. Every data point corresponds to twenty simulations with different seeds for the random number generator. The average shape is plotted, with the length of the error bar corresponding to the standard error, calculated from those simulations which lead to an aggregate. Curves for the Roche ellipsoid are calculated using (1) the maximum packing density for the identical particle aggregate, which leads to $0.74 \times 900\,\mathrm{kg\,m^{-3}}$, (2) $\rho = 0.8 \times 900\,\mathrm{kg\,m^{-3}}$ to reflect the average packing density 0.8 with size distribution simulations, and (3) $\rho = 900\,\mathrm{kg\,m^{-3}}$ as that is the internal density of single particle. For clarity, only the last one is plotted to the lower diagram, as the other two would be very close to the $900\,\mathrm{kg\,m^{-3}}$ curve. The r_p values marked in the lower axes of the diagrams correspond to pairs of identical particles with $\rho = 900\,\mathrm{kg\,m^{-3}}$. Shapes and distances for the moons are from Porco et al. (2006).

aggregates made up with particles that have a size distribution, and the last one for the internal density of the particles. The volume densities for the aggregates we use for collisions can be found in Table 1.

3.2. How to measure the mass change of target aggregates

In three-body integrations there are two bodies orbiting the central object, and there are just two possible post-collisional outcomes, capture or non-capture. For example, Ohtsuki (1993) defines for each mutual orbit $p_\mathrm{col}(e, i, b, \tau, \omega)$ by 1 for collisional orbits and 0 otherwise, and $p_\mathrm{cap}(e, i, b, \tau, \omega)$ by 1 for collisions when particles stick together after the impact and 0 otherwise, where e, i, b, τ, and ω are the orbital elements of the relative orbit (τ and ω stand for the phases of radial and vertical epicycles). He then calculates the capture probability by using the following collisional rate

$$P_\mathrm{col} = \int p_\mathrm{col}(e, i, b, \tau, \omega)\frac{3}{2}|b|\,\mathrm{d}b\,\frac{\mathrm{d}\tau\,\mathrm{d}\omega}{(2\pi)^2} \tag{13}$$

(Nakazawa et al., 1989) and the rate of capture

$$P_\mathrm{cap} = \int p_\mathrm{cap}(e, i, b, \tau, \omega)\frac{3}{2}|b|\,\mathrm{d}b\,\frac{\mathrm{d}\tau\,\mathrm{d}\omega}{(2\pi)^2}. \tag{14}$$

Then the probability of capture $C(e, i)$, is defined by the conditional probability

$$C(e, i) = P_\mathrm{cap}(e, i)/P_\mathrm{col}(e, i). \tag{15}$$

The difference in the case of colliding aggregates is that there is a continuum of outcomes: in addition to cases when the target aggregate disintegrates totally or contains both its own mass and the whole impactor mass, the mass can be anything in between those extremes; thus p_cap cannot be defined in the same manner as above. Besides actual physical impacts we also study the effect of close encounters since they can also disrupt the target aggregate. Therefore p_col is not well defined and we need a different normalization for this interaction frequency.

We shall proceed by using a measure of capture that takes into account the continuous distribution of impact outcomes. Also, a convenient way to obtain a rough estimate for the impact frequency is to assume the planar case with impacts coming from circular orbits and to ignore self-gravity. Then we get the impact frequency for the target particle

$$\omega_\mathrm{c} = \int_{-(R_1+R_2)}^{R_1+R_2} n\frac{3}{2}\Omega|x|\,\mathrm{d}x = n\frac{3}{2}\Omega(R_1 + R_2)^2, \tag{16}$$

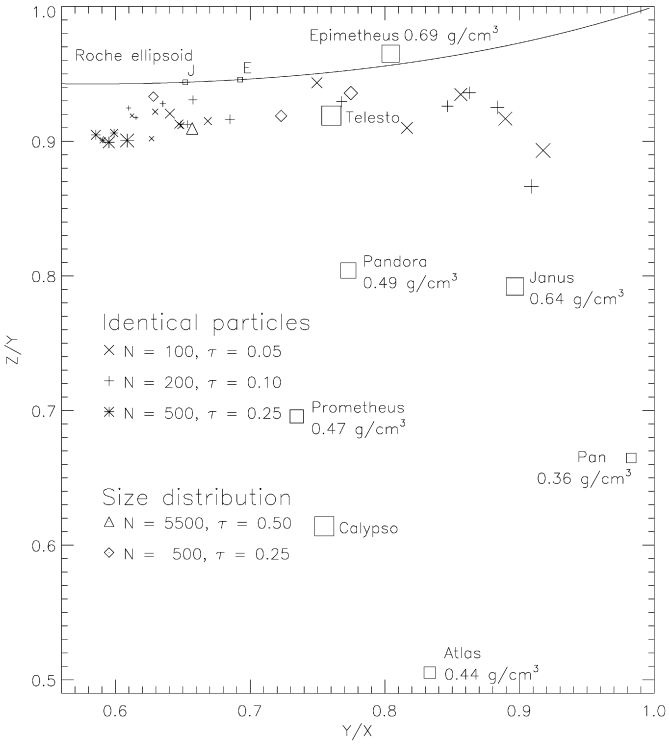

Fig. 5. *Shape of the aggregates forming via gradual growth.* Z/Y vs Y/X ratios, where X, Y, and Z are the main axes of the ellipsoid fitted to the aggregate. Data points are averages over twenty simulations with different seeds for the random number generator, leading to formation of an aggregate. The Roche line is calculated from theoretical Y/X and Z/Y ratios. On the Roche curve the J and E refer to Roche ellipsoids with Janus' (0.64 g cm^3) and Epimetheus' (0.69 g cm^{-3}) internal density. Shapes and internal densities for the moons are from Porco et al. (2006).

where R_1 and R_2 are the radii of target and impactor, respectively, and n is the surface density of impactors. This can be compared to the actual impact frequency in the non-gravitating case (thick 3D systems): $\omega_c = 13.9n(R_1 + R_2)^2$ impacts per orbit (Salo, 1992a), corresponding to $\omega_c = 2.21n\Omega(R_1 + R_2)^2$. In practice, the impact frequency is a few times larger due to gravitational focusing.

Our original standard target aggregate has 500 particles. After the impact the number of particles in the three biggest remaining fragments are measured, no matter where the particles originate. Then comparing the biggest one to the original target aggregate gives the mass change.

The net increase or decrease of mass per impact can be written as $F = (m_{\text{final}} - m_{\text{initial}})/m_{\text{initial}}$. F depends on impact parameter b, thus we get the effective average mass change per impact

$$c_{\text{ag}} = \frac{\int_{-\infty}^{\infty} F(|b|) n \frac{3}{2}\Omega |b|\,\mathrm{d}b}{\int_{-(b_1+b_2)}^{b_1+b_2} n \frac{3}{2}\Omega |b|\,\mathrm{d}b}, \tag{17}$$

where b_1 and b_2 correspond to R_1 and R_2 in Hill units. As the aggregates are not spheres the effective radius $r_{\text{eff}} = (XYZ)^{1/3}$ has been used as R_1 and R_2 for the target and the impactor aggregates. Although our normalization is somewhat arbitrary, it provides simple means to convert c_{ag} to accretion rate versus time, for a given n.

Table 1
Properties of impactor aggregates

N_{tot}	N_{impactor}	Y/X	Z/Y	Volume density	Remarks [a]
1000	500	0.587	0.912	0.69	Standard aggregate[b]
750	250	0.556	0.915	0.69	$\mu = 2$
600	100	0.576	0.928	0.70	$\mu = 5$
550	50	0.611	0.890	0.74	$\mu = 10$
1000	500	0.584	0.911	0.69	$\epsilon_{\text{n}} = 0.1$[c]
1000	500	0.585	0.911	0.69	$k_{\text{f}} = 0.1$[d]
1000	500	0.712	0.905	0.83	Size distribution[e]
1000	500	0.456	0.935	0.69	Elongated aggregate
1000	500	0.587	0.912	0.69	Standard aggregate
1000	500	0.973	0.858	0.74	Roundish aggregate

[a] Difference compared to the standard aggregate with $\mu = 1$, $k_{\text{f}} = 0$, $\epsilon_{\text{n}}(v_{\text{n}})$ and identical particles.
[b] Target aggregate for all μ's.
[c] Standard aggregate run continued for 10 orbits with modified ϵ and a.
[d] Standard aggregate run continued for 10 orbits with modified k_{f} and a.
[e] $q = 3$, 0.5 m $< r <$ 5.0 m.

4. Accretion probability in aggregate collisions

Impacts between different sized aggregates was one of the main interests of this study. Barbara and Esposito (2002) assume a critical mass ratio of $\mu \sim 100$, above which there is total accretion and below which complete disruption. They assumed this to be valid at the F ring distance $a = 140{,}000$ km. This critical mass ratio corresponds to $r_{\text{p}} < 2/3$ for $\rho = 900\ \text{kg m}^{-3}$. Their criterion also satisfies the Canup and Esposito's (1995) criterion for accretion, $r_{\text{p}} \lesssim 0.691$.

4.1. Mass ratio

We made simulations with aggregate mass ratios from 1 to 10. The smaller aggregates had the same shape as our standard target aggregate. Different mass ratios studied are listed in Table 1. We did not have to go to a wider range to see that the outcome of a collision for our chosen interval $a =$ 135,000–145,000 km, can already vary from total destruction of the target aggregate to complete accretion of aggregates. The net mass change of the target aggregate calculated with Eq. (17) for different r_{p}'s is shown in Fig. 6. There is net destruction with all studied mass ratios at distance 135,000 km, whereas for 145,000 km all mass ratios lead to accretion. The transition zone from destructive collisions to accreting ones is thus quite narrow. At the F ring distance 140,000 km, we have both net accretion and net disruption, depending on the mass ratio of colliding aggregates. For the net accretion distance (145,000 km) the c_{ag} is bigger for bigger impactor mass, but increasing the impactor mass tenfold does not increase c_{ag} tenfold. At 135,000 km, where the collisions end up disrupting the aggregates, roughly the bigger impactor aggregate the more disruptive the outcome is.

A summary of these runs is given in Table 2.

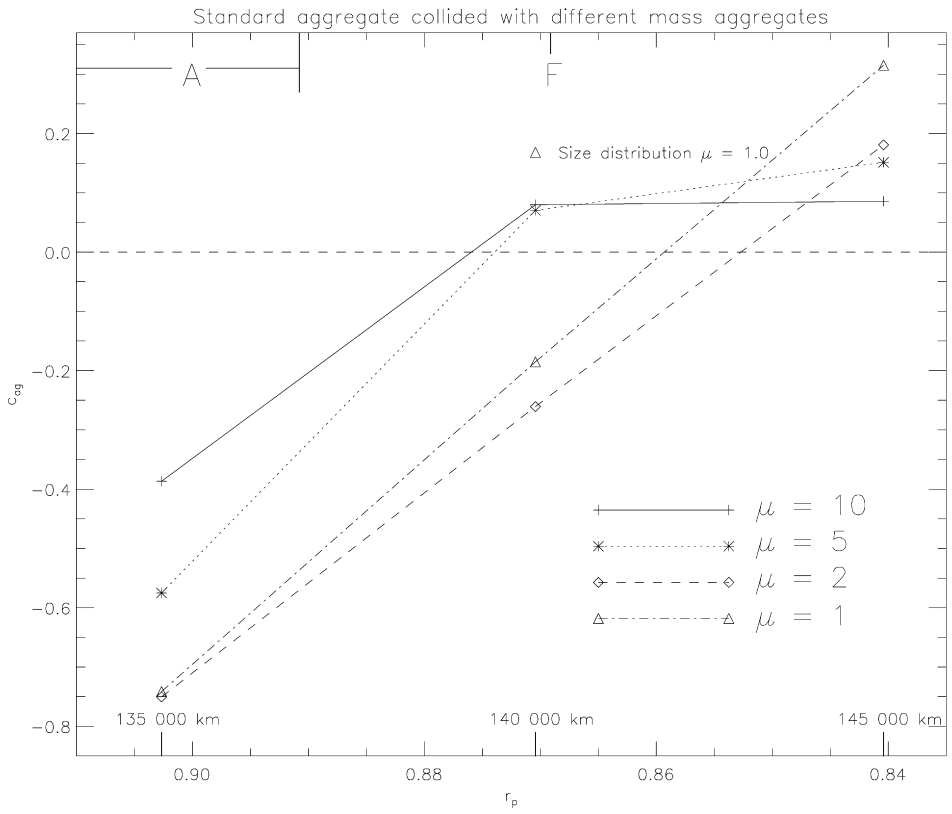

Fig. 6. *Mass change in aggregate impacts*. Accretion rate for collisions between particle aggregates with different mass ratios and particle properties. On the horizontal axis are the distances for collisional simulations that were conducted; also included are the r_p values for the identical particle pair with $\rho = 900\,\mathrm{kg\,m^{-3}}$. On the vertical axis is the c_{ag} (see Eq. (17)). The target aggregate has always 500 particles and the impactor aggregate has 500, 250, 100, and 50 for mass ratios 1, 2, 5, and 10, respectively. The unattached point at 140,000 km is for $\mu = 1.0$ but particles building up the aggregate have a size distribution ($q = 3$, 0.5 m $< r <$ 5 m).

4.2. Elasticity models

Besides Bridges et al.'s (1984) velocity-dependent coefficient of restitution $\epsilon_n(v_n)$, a constant coefficient of restitution $\epsilon_n = 0.1$ has been studied as well. The same standard aggregate was used but the elasticity model was changed. This was done to prevent the effect of shape stepping in. From previous results, e.g., Karjalainen and Salo (2004), we expected simulations with $\epsilon_n = 0.1$ to be more probable to accrete than the ones with $\epsilon_n(v_n)$. We took the original standard aggregate and changed its velocity-dependent coefficient of restitution to a constant one and simulated the aggregate in isolation for 10 orbits, to let it to settle to a possible new form. It turned out that there was practically no change at all in the shape and volume density (see Table 1). Then this aggregate, with a new elasticity law was collided with another identical aggregate ($\mu = 1$). The outcome of using constant $\epsilon_n = 0.1$ compared to $\epsilon_n(v_n)$ leads to increased accretion at the studied distance $a = 140{,}000$ km ($c_{ag} = 0.214$ compared to -0.185 for the standard case with Bridges' formula). Assuming that the radial dependence of c_{ag} is similar to that in the standard case would suggest that the limit between destructive/accreting impacts ($c_{ag} = 0$) is shifted inward by about 4000 km. This is in qualitative agreement with Karjalainen and Salo (2004), where the accretion distance was shifted 6000 km inward by the change from velocity-dependent coefficient of restitution to a constant 0.1.

4.3. Coefficient of friction

Collisional dissipation is enhanced by friction, thus friction can have a significant role in particle aggregation. We studied the role of friction in a similar manner as that of elasticity: we took the standard aggregate and changed this time the coefficient of friction k_f from 0.0 to 0.1, and let the aggregate again to evolve for 10 orbits. Again there was no significant mass rearrangement, see Table 1. After this the aggregate was collided with an identical aggregate. The net result for $a = 140{,}000$ km is increased accretion corresponding to 2000–3000 km inward shift to our standard run with no friction. In gradual growth the inward shift for cases where there was accretion was 5000 km (see Karjalainen and Salo, 2004, Fig. 8b).

4.4. Size distribution

Inclusion of a size distribution moved the distance of the onset of accretion about 10,000 km towards the planet (Karjalainen and Salo, 2004). This means that there should be more gradually accreted aggregates in 135,000–145,000 km, the region that we are interested in. Similarly, colliding two aggregates with a size distribution ($\mu = 1$) we obtain increased accretion compared to aggregates composed of identical particles. Extrapolating the test case for 140,000 km we can estimate that the limit $c_{ag} = 0$ is shifted ~5000 km inward compared to the standard case (see Fig. 6).

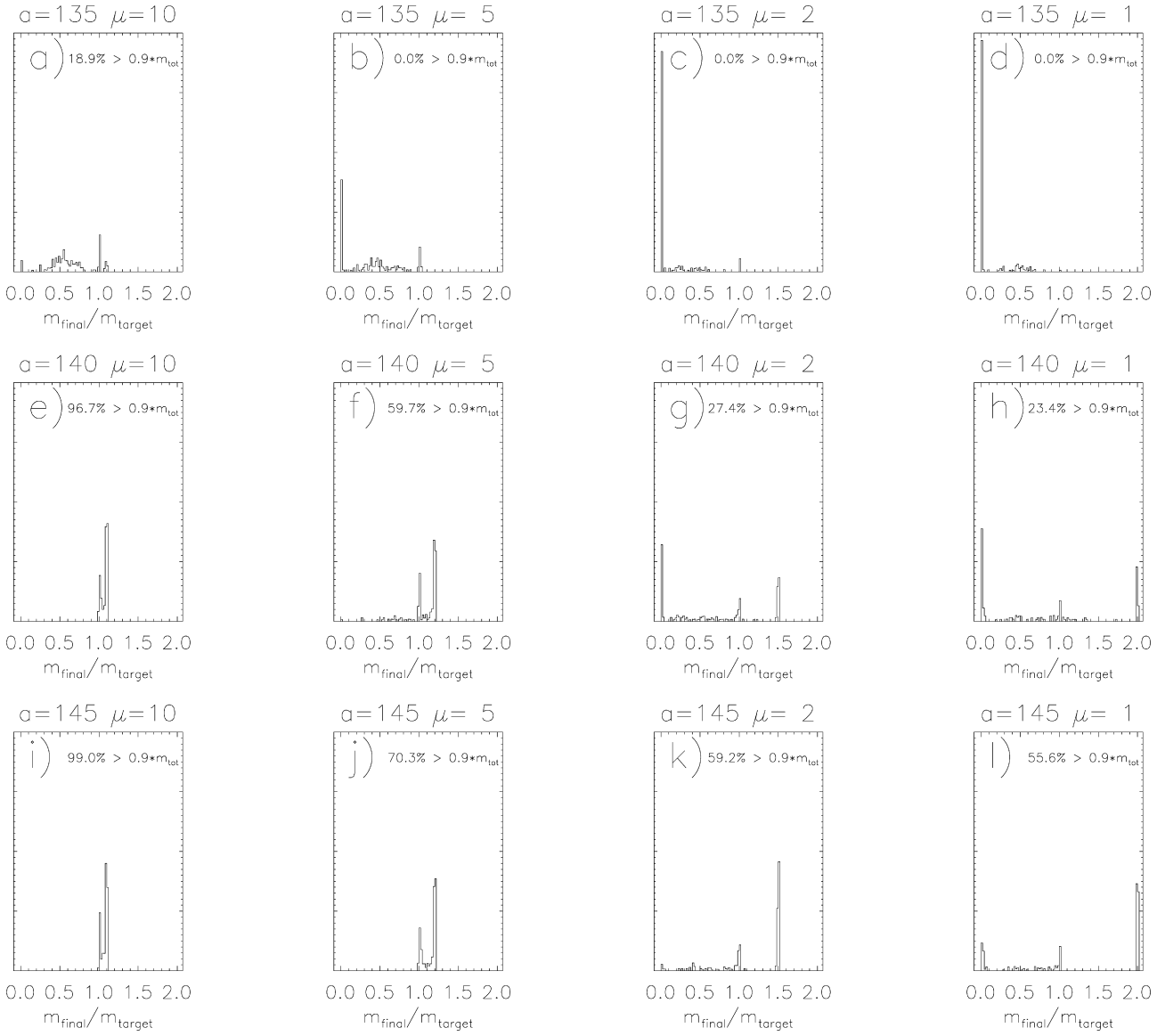

Fig. 7. *Mass distribution after the collision*. These histograms show the mass distribution after the collision of aggregates. On the horizontal axis is the mass of the biggest remaining particle group. All simulations for different b's are shown, with appropriate weight proportional to b. The percentage of cases where the mass of the final aggregate is more than 90% of the total mass is shown in each plot. Histograms (a)–(l) show the mass ratio simulations with three different distances, while (m)–(r) show the effects of friction, constant coefficient of restitution, size distribution and the shape of the aggregate.

4.5. Comparison to three-body calculations

Above we have estimated the boundary between regions of net disruption and net accretion. To compare our aggregate simulations more directly to three-body calculations we also made a comparison using the same formulas as in three-body calculations, i.e., Eqs. (13)–(14). In order to do so we need to specify what is now meant by capture and non-capture. Also, we would need to use the actual impact rate. In order to get a reasonable approximation we define that where more than 90% of the particles are attached to the post-impact target aggregate it is considered as a capture event. It turns out that for the impact frequency no large error is made if we assume that all impact parameter values used lead to a collision. In Fig. 7 one can see the histograms of the outcomes of collision with mass ratios of colliding aggregates from 1 to 10 and distances from 135,000 to 145,000 km. In every histogram there is marked the percentage of cases where the mass of the final aggregate is more than 90% of the combined mass: this fraction will be called $c'_{\rm ag}$. Now we can calculate the $r_{\rm p}$ values for the aggregate pairs to compare these results with Ohtsuki (1993). Also, we will use $c'_{\rm ag} > 50\%$ as an accretion criterion (see Fig. 8). In Table 3 one can find a summary of the results.

We can see that while $r_{\rm p}$'s go from 0.83 to 1.02 the $c'_{\rm ag}$ drops from 1 to 0. This can be compared to Ohtsuki's (1993) Fig. 8, where there is a steep change between $r_{\rm p}$'s 0.7 to 0.8 with his calculations for $\epsilon_{\rm n} = 0.5$. Qualitatively our results are similar, as can be seen from the $c'_{\rm ag}$ values for different $r_{\rm p}$'s in Table 3. However, we seem to get higher capture probabilities, and a transition from capture to non-capture in an even shorter $r_{\rm p}$ in-

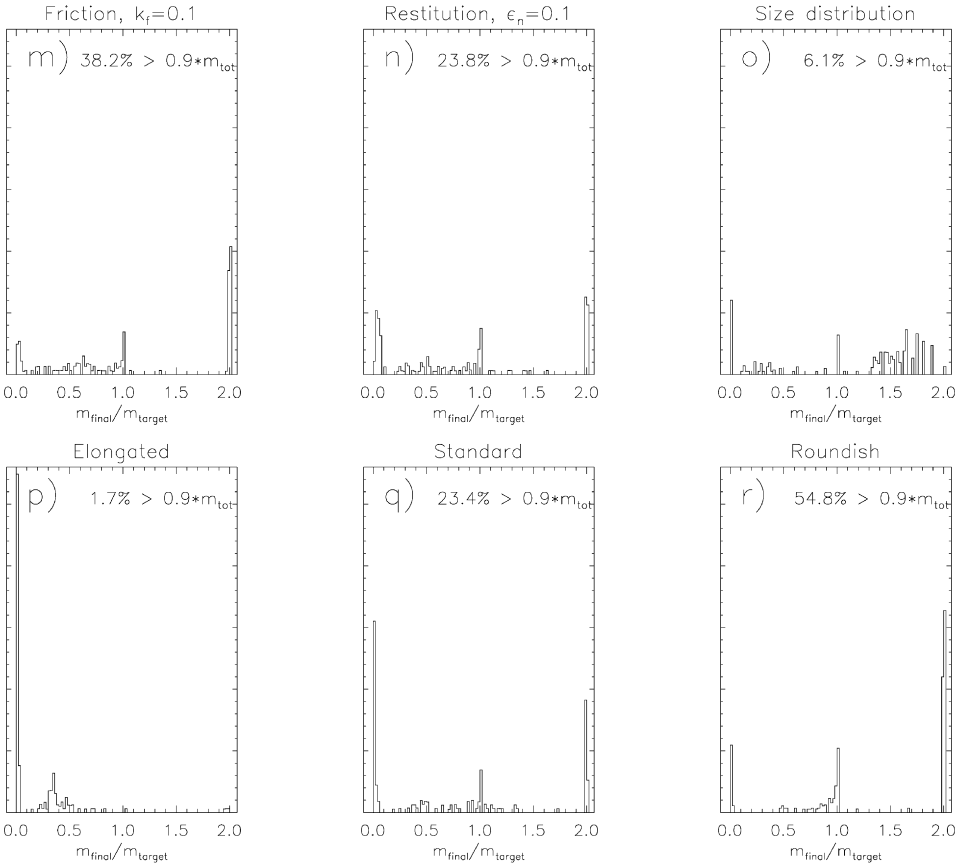

Fig. 7. (*continued*)

Table 2
Mass change after the impact between two aggregates

μ	Distance a [km]	c_{ag}	%[a]	Remarks
1	135,000	−0.742	0.0	
	140,000	−0.185	47.6	
	145,000	0.315	66.3	
2	135,000	−0.751	5.4	
	140,000	−0.261	45.0	
	145,000	0.181	69.6	
5	135,000	−0.575	9.9	
	140,000	0.070	81.9	
	145,000	0.152	97.3	
10	135,000	−0.387	16.6	
	140,000	0.080	96.6	
	145,000	0.086	98.9	
1	140,000	0.214	37.7	$\epsilon_n = 0.1$
1	140,000	0.088	46.9	$k_f = 0.1$
1	140,000	0.168	71.2	Size distribution[b]
1	140,000	−0.728	3.60	Elongated
1	140,000	−0.185	47.6	Standard
1	140,000	0.373	68.4	Roundish

[a] Percentage of cases when $m_{final}/m_{target} > 1.0$.

[b] $q = 3$, 0.5 m $< r <$ 5.0 m.

terval than in Ohtsuki's (1993) Fig. 8. Thus it seems that the r_p criterion band on three-body integrations of solid spherical particles is not fully accurate for aggregate impacts.

Table 3
Comparison to three-body calculations

a [km]	μ	Volume density	r_p[a]	c'_{ag} [%]
135,000	1	0.69	1.02	0
140,000	1	0.69	0.99	30
145,000	1	0.69	0.95	59
135,000	2	0.69	1.01	0
140,000	2	0.69	0.97	35
145,000	2	0.69	0.94	61
135,000	5	0.70	0.96	0
140,000	5	0.70	0.92	60
145,000	5	0.70	0.89	70
135,000	10	0.74	0.89	19
140,000	10	0.74	0.86	97
145,000	10	0.74	0.83	99

[a] r_p value for the target–impactor pair, using the effective radii $r_{eff} = (XYZ)^{1/3}$ for the target aggregate's and the impactor aggregate's physical radius in Eq. (1).

Fig. 8 shows the accretion region for spherical particles and for the aggregates. The critical mass ratio 100 used by Barbara and Esposito (2002) is clearly in the area where there is accretion according to Ohtsuki (1993) and Canup and Esposito (1995). Our simulations are only for mass ratios from 1 to 10, but they give clearly different results compared to the beforementioned criteria as our colliding aggregates start to merge already around 140,000 km while the three-body criteria give

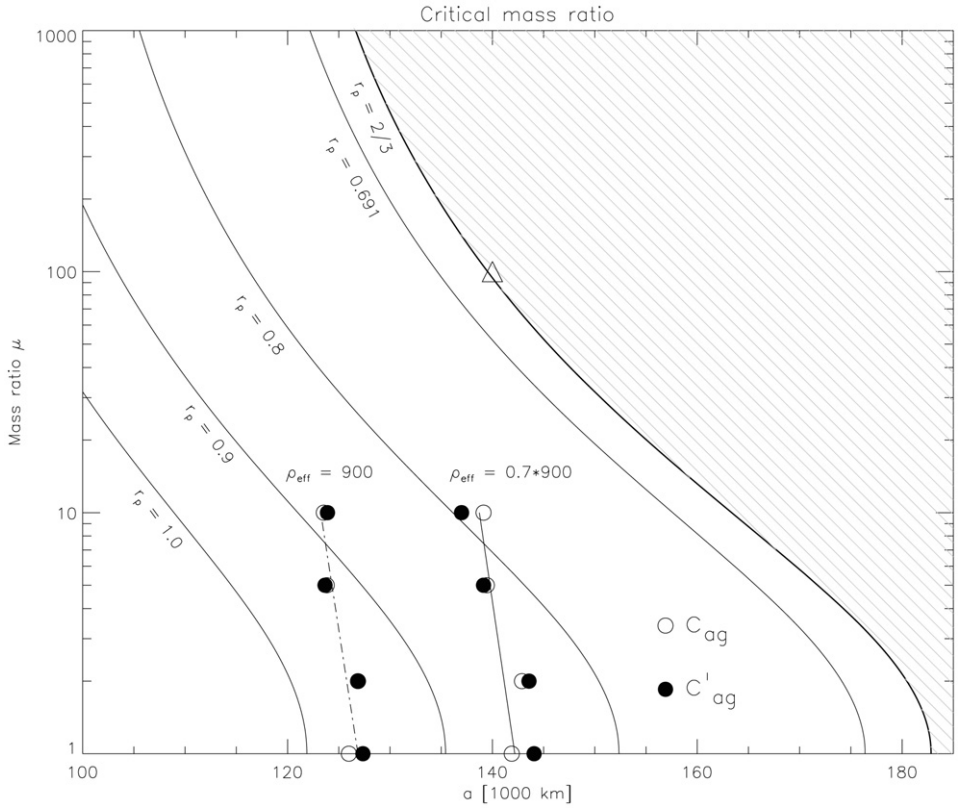

Fig. 8. *The critical mass ratio*. The region of accretion as a function of distance and mass ratio for $\rho = 900\,\mathrm{kg\,m^{-3}}$. The thick line indicates the Ohtsuki's (1993) criterion for accretion $r_\mathrm{p} \leqslant 2/3$, the shaded area denotes the accretion zone. Canup and Esposito (1995) require $r_\mathrm{p} \lesssim 0.691$ for capture. The triangle denotes the criterion Barbara and Esposito (2002) use for $a = 140{,}000$ km, corresponding to $r_\mathrm{p} = 2/3$ curve. Our simulation results are shown with open circles for $c_\mathrm{ag} = 0$ as the border between net disruption and net accretion, and closed circles denoting the $c'_\mathrm{ag} = 50\%$ as a border between net disruption and net accretion. We have increased the internal density of the aggregate to mimic single solid ice particles (with filling factor of 1, compared to ∼0.7 with aggregates), thus $\rho_\mathrm{eff} = 900\,\mathrm{kg\,m^{-3}}$. The lines are fitted to data from using $c_\mathrm{ag} = 0$ criterion. For comparison also r_p's 0.8, 0.9, and 1.0 are plotted.

accretion between 155,000 and 185,000 km, for $\mu = 1$–10. For our standard aggregate the use of bigger mass ratios than we used in our simulations would mean smaller impactors, and thus it would get closer and closer to the test particle case and therefore it would be safe to assume that the bigger mass ratios would give us similar results as the criteria of Ohtsuki (1993) and of Barbara and Esposito (2002). An important difference between three-body calculations and aggregate collisions has to be taken into account, namely the volume density. With single particles it is one and thus the effective internal density is ρ. With aggregates the volume density is less than one (∼0.7–0.8, depending on whether identical particles or a size distribution is used) and this can be taken into account, which would make the difference from three-body calculations even bigger, as can be seen by comparing the solid straight line that denotes the $\rho_\mathrm{eff} = 0.7 \times 900\,\mathrm{kg\,m^{-3}}$ to the dashed line that denotes $\rho_\mathrm{eff} = 900\,\mathrm{kg\,m^{-3}}$ in Fig. 8. The crucial reason why the collision of aggregates gives so much more accretion compared to the collision of solid particles is that the shape of the forming aggregate evolves in aggregate collisions: the particles of the original aggregates can coalesce into a single ellipsoidal body (see the middle row of Fig. 2) leading to stronger gravitational binding than in the case of the two spherical particles retaining their identity and shape.

5. Conclusions and discussion

We made a set of local N-body simulations to study the break-up and accretion of ring particle aggregates. The simulations took into account the mutual impacts between particles as well as gravitational forces. Our main interest was the outcome of the collision of aggregates at various distances.

Our simulations support the standard assumption of having a critical mass ratio between the particles or aggregates that limits which collisions lead to accretion and which to disruption, like the one used by Barbara and Esposito (2002). However, the ratio of ∼100 that they use (from the three-body criterion), for the F ring distance is not strictly supported by our simulations. One should take the impact parameter in account along with the distance to the central object (and the internal density of ring particles). With different impact parameters one can get either accretion or destruction of identical colliding aggregates. Averaging over the impact parameter range (and assuming circular initial orbits) the collisions between aggregates that have mass ratios from 1 to 10 end up destructive at 135,000 km distance. At 145,000 km there is net accretion with all before-mentioned mass ratios. The intermediate distance studied, 140,000 km, is more complicated as it is in the transition zone from destructive to accreting collisions when the mass ratio varies between 1

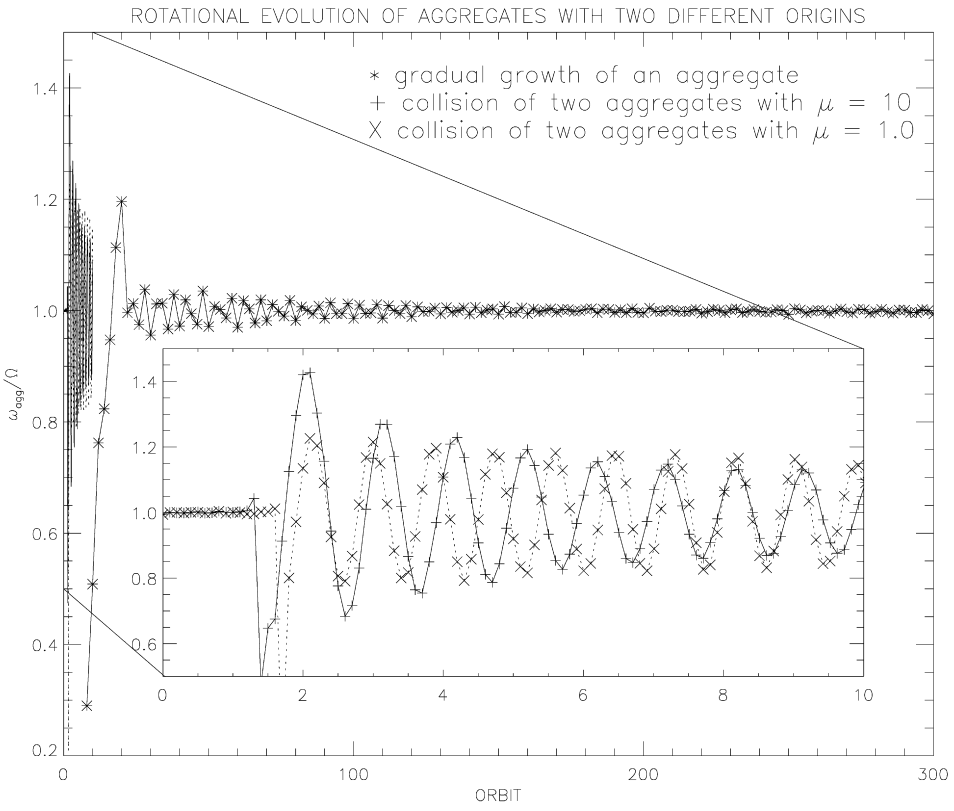

Fig. 9. *Evolution of the aggregate rotation*. Comparison between aggregates forming via gradual growth, and those forming via merging of two colliding aggregates. Both cases evolve toward synchronous rotation.

and 5. As a conclusion we can say that for the F ring region a critical μ is likely to exist, but its exact value is much harder to define.

In order to see the effect of increased dissipation in impacts the constant coefficient of restitution $\epsilon_n = 0.1$ was studied besides $\epsilon_n(v_n)$ from Bridges et al. (1984). Constant $\epsilon_n = 0.1$ behaves similarly with both gradual growth (Karjalainen and Salo, 2004) and aggregate collisions, giving an inward shift of about 6000 and 4000 km, respectively, as compared to $\epsilon_n(v_n)$. The distances are from accretion zone in gradual growth and c_{ag} in aggregate collisions. The effect of friction was studied by using the friction coefficient $k_f = 0.1$. Including friction corresponds to about 2000 km inward shift for the distance when comparing the c_{ag} values. This agrees with Karjalainen and Salo's (2004) results, where the distance where aggregates form in simulations with $k_f = 0.1$ is 5000 km closer to Saturn than without friction. Using a size distribution in the particles that form the colliding aggregates increases the probability of accretion. The difference where gradually grown aggregates always form for aggregates with and without a size distribution is about 6000 km, the distance for a size distribution being 140,000 km (see Karjalainen and Salo, 2004, Fig. 9a). Using the same size distribution for ring particles constituting the aggregate–aggregate collisions gives c_{ag} that is comparable to what identical particles would give at distance 143,000 km, see Fig. 6 with $\mu = 1.0$.

To summarize the comparison between the results of colliding aggregates and gradually grown aggregates with the same initial parameters, i.e., $\epsilon_n(v_n)$, identical particles and no friction: if we change $\epsilon_n(v_n)$ to $\epsilon_n = 0.1$ or identical particles to a size distribution or $k_f = 0.0$ to $k_f = 0.1$ we get more accretion for a given distance. In the gradual growth case of Karlajainen and Salo's (2004) paper, we compare the cases when there are always aggregates forming, and with aggregate collisions' case we can compare the c_{ag} values. The difference in terms of distance to planet is of the order of few thousands of kilometers but with aggregate collisions it is less than with gradual growth.

The rotational state approaches the synchronous state whether the aggregate is formed via gradual accretion or by a coalescence of two colliding aggregates (see Fig. 9). The rotational state of the aggregate that is formed after the collision is independent of the impact parameter. Neither the distance nor the mass ratio of colliding aggregates seems to have any effect on the rotation. The collisions might lead to an anomalous temporary spin state of the target aggregate but the spin then evolves to synchronous rotation.

The shape of the aggregate is a vital factor deciding whether the collision leads to accretion or destruction. For the distance range $a = 135{,}000$–$145{,}000$ km the gravitationally bound aggregates that have formed independently via cumulative accretion have an average shape which allows either accretion or destruction, depending on b. Single aggregates can form also with very elongated form and these get destroyed easily; then on the other hand round aggregates form too and they are far more difficult to destroy. Table 2 lists also the c_{ag} values for these more extreme shapes for $a = 140{,}000$ km. They are not

included in Fig. 6 for clarity but one can see that the shape is a big factor and the data points for elongated and roundish aggregates would be at extremes in Fig. 6.

A comparison to three-body accretion calculations was made by using a crude criterion for simplifying the aggregate impact outcomes as captures and non-captures (capture in the case if 90% of the post-impact mass is in the target aggregate). This way we could compare to the accretion criterion used by Ohtsuki (1993), Canup and Esposito (1995), and Barbara and Esposito (2002). The effect of shape is evident also when comparing our results of aggregate collisions to three-body calculations. Using a three-body criterion to decide the critical mass ratio for the outcome of an aggregate collision simply fails with the small μ's studied here. For bigger μ's it is more realistic as then the situation is closer to a test particle case when the mass of the smaller aggregate is negligible compared to the bigger aggregate's mass (see Fig. 8). The reason for the very different accretion boundary, in terms of r_p, for aggregate collisions compared to collisions between two particles is the internal mobility of the aggregates. In three-body calculations, when particles collide they keep their shape, while in collisions between two aggregates the shape changes a lot and thus permits accretion more easily.

Ohtsuki's (1993) three-body trajectory integration results for accretion in Saturn's rings are supported by our N-body simulations, taking into account that his results are for individual particles and ours for aggregates. Our c'_ag is calculated in the same way as Ohtsuki's probability of capture C. Qualitatively the results agree well as for r_p from 0.83 to 1.02 we get the steep drop for probability c'_ag, from 1 to 0 just like in Ohtsuki's (1993) Fig. 8, for slightly smaller r_p's. However, the use of r_p in the case of aggregate collisions is not as clear as with single spherical particles.

Porco et al. (2006) discuss the possibility that Saturn's small satellites Pan, Atlas, Prometheus, Pandora, Janus, Epimetheus, Telesto, and Calypso might be rubble piles formed by accretion. Their shape, i.e. the axis ratios Y/X and Z/Y are shown in Fig. 5 and comparing them to our simulations shows that while our results lie quite close to Roche ellipsoids, the moons (excluding Epimetheus and Telesto) are further away from it. As our results are from gradual growth of particle aggregates and there is no tensile strength, we can rule out this pure gravitational aggregate possibility from the origin of the moons. At least there should be a mechanism that makes the moons (not including Telesto and Epimetheus) flatter. Epimetheus seems to have the Roche ellipsoid shape but when we take into account its distance and internal density we see that if it were an idealized Roche ellipsoid it should not be as round as it is. The Roche ellipsoid shapes can be calculated for Janus and Epimetheus as we know their distance and internal density, while for other moons either the density is not known or it is so small that no stable Roche ellipsoid would exist for their distance.

Our simulations were restricted to circular initial orbits of the encountering aggregates. A natural follow-up would be to take into account the eccentricities and inclinations of the impactors, which however would complicate the problem considerably (integrations over impact parameter would need to be augmented by 4-dimensional integration over velocity space). However, in the case of colliding aggregates the assumption of circular orbits is not too restrictive because the simulations have shown that bigger particles and especially aggregates have smaller inclinations and eccentricities. Also, our modeling of collisions does not include adhesion and it would be very interesting to see how it affects the accretion rate. Even a small adhesive force might have a big effect on the sticking probabilities of ring particles. However, adhesion is a kind of on/off force that it has an effect only when particles are attached to each other, different from gravity, that is effective even when the particles are not touching each other.

So far the simulations have been made with spherical particles. It would be interesting to see how different shapes of the particles would change the outcome of the collisions, using for example polyhedrons like Korycansky and Asphaug (2006). Re-modeling the mass and velocity evolution of a colliding swarm of particles like Barbara and Esposito (2002) but using a refined smaller critical mass estimate would be a natural follow-up too.

Acknowledgments

This work was supported by the Academy of Finland, Space Institute at the University of Oulu and Magnus Ehrnrooth foundation. I would like to thank Heikki Salo for his many contributions to this work, Ryuji Morishima for his comments on the manuscript and the referees Anthony Dobrovolskis and Larry Esposito for their detailed and helpful reviews.

References

Albers, N., Spahn, F., 2006. The influence of particle adhesion on the stability of agglomerates in Saturn's rings. Icarus 181, 292–301.

Barbara, J.M., Esposito, L.W., 2002. Moonlet collisions and the effects of tidally modified accretion in Saturn's F ring. Icarus 160, 161–171.

Bridges, F.G., Hatzes, A., Lin, D.N.C., 1984. Structure, stability and evolution of Saturn's rings. Nature 309, 333–335.

Bridges, F.G., Supulver, K.D., Lin, D.N.C., 2001. Energy loss and aggregation processes in low speed collision of ice particles coated with frosts or methanol/water mixtures. In: Pöschel, T., Luding, S. (Eds.), Granular Gases. In: Lecture Notes in Physics, vol. 564. Springer-Verlag, Berlin, pp. 153–183.

Canup, R.M., Esposito, L.W., 1995. Accretion in the Roche zone: Coexistence of rings and ringmoons. Icarus 113, 331–352.

Chandrasekhar, S., 1969. Ellipsoidal Figs of Equilibrium. The Silliman Foundation Lectures. Yale Univ. Press, New Haven.

Cuzzi, J.N., Burns, J.A., 1988. Charged particle depletion surrounding Saturn's dusty F ring: Evidence for a moonlet belt? Icarus 74, 284–324.

Ida, S., Nakazawa, K., 1989. Collisional probability of planetesimals revolving in the solar gravitational field. III. Astron. Astrophys. 224, 303–315.

Karjalainen, R., Salo, H., 2004. Gravitational accretion of particles in Saturn's rings. Icarus 172, 328–348.

Korycansky, D.G., Asphaug, E., 2006. Low-speed impacts between rubble piles modeled as collections of polyhedra. Icarus 181, 605–617.

Marouf, E.A., Tyler, G.L., Zebker, H.A., Simpson, R.A., Eshleman, V.R., 1983. Particle size distributions in Saturn's rings from Voyager 1 radio occultation. Icarus 54, 189–211.

Meinke, B.K., Esposito, L.W., Colwell, J.E., 2006. Moonlets and clumps in Saturn's F ring. Bull. Am. Astron. Soc. 38. Abstract 47.02.

Morishima, R., Salo, H., 2004. Spin rates of small moonlets embedded in planetary rings. I. Three-body calculations. Icarus 167, 330–346.

Murray, C.D., Dermott, S.F., 2000. Solar System Dynamics. Cambridge Univ. Press.

Nakazawa, K., Ida, S., Nakagawa, Y., 1989. Collisional probability of planetesimals revolving in the solar gravitational field. I. Basic formulation. Astron. Astrophys. 220, 293–300.

Ohtsuki, K., 1993. Capture probability of colliding planetesimals: Dynamical constraints on accretion of planets, satellites, and ring particles. Icarus 106, 228–246.

Porco, C.C., Weiss, J.W., Thomas, P.C., Richardson, D.C., Jacobson, R.A., Spitale, J., 2006. Physical characteristics and possible accretionary origins for Saturn's small satellites. Lunar Planet. Sci. 37. Abstract 2289.

Poulet, F., Sicardy, B., Nicholson, P., Karkoschka, E., Caldwell, J., 2000. Saturn's ring-plane crossing of August and November 1995: A model for the new F-ring objects. Icarus 144, 135–148.

Salo, H., 1991. Numerical simulations of dense collisional systems. Icarus 90, 254–270.

Salo, H., 1992a. Numerical simulations of dense collisional systems. II. Extended distribution of particle sizes. Icarus 96, 85–106.

Salo, H., 1992b. Gravitational wakes in Saturn's rings. Nature 359, 619–621.

Salo, H., 1995. Simulations of dense planetary rings. III. Self-gravitating identical particles. Icarus 117, 287–312.

Seiß, M., Spahn, F., Sremčević, M., Salo, H., 2005. Structures induced by small moonlets in Saturn's rings: Implications for the Cassini mission. Geophys. Res. Lett. 32. L11205.

Showalter, M.R., 1998. Detection of centimeter-sized meteoroid impact events in Saturn's F ring. Science 282, 1099–1102.

Showalter, M.R., 2004. Disentangling Saturn's F ring. I. Clump orbits and lifetimes. Icarus 171, 356–371.

Supulver, K.D., Bridges, F.G., Lin, D.N.C., 1995. The coefficient of restitution of ice particles in glancing collisions: Experimental results for unfrosted surfaces. Icarus 113, 188–199.

Tiscareno, M.S., Burns, J.A., Hedman, M.M., Porco, C.C., Weiss, J.W., Dones, L., Richardson, D.C., Murray, C.D., 2006. 100-meter-diameter moonlets in Saturn's A ring from observations of 'propeller' structures. Nature 440, 648–650.

Weidenschilling, S.J., Chapman, C.R., Davis, D., Greenberg, R., 1984. Ring particles: Collisional interactions and physical nature. In: Greenberg, R., Brahic, A. (Eds.), Planetary Rings. Univ. of Arizona Press, Tucson, pp. 367–415.

Wisdom, J., Tremaine, S., 1988. Local simulations of planetary rings. Astron. J. 95, 925–940.